HHS Public Access

A 3D high resolution *ex vivo* white matter atlas of the common squirrel monkey (*Saimiri sciureus*) based on diffusion tensor imaging

Yurui Gao[a,b], Prasanna Parvathaneni[c], Kurt G. Schilling[a,b], Feng Wang[b,d], Iwona Stepniewska[e], Zhoubing Xu[c], Ann S. Choe[a,b], Zhaohua Ding[a,b,c,d], John C. Gore[a,b,c,d], Li Min Chen[b,d], Bennett A. Landman[a,b,c,d,*], and Adam W. Anderson[a,b,d]

[a]Biomedical Engineering, Vanderbilt University, Nashville, TN USA

[b]Institute of Imaging Science, Vanderbilt University, Nashville, TN USA

[c]Electrical Engineering and Computer Science, Vanderbilt University, Nashville, TN USA

[d]Radiology and Radiological Sciences, Vanderbilt University, Nashville, TN USA

[e]Psychology, Vanderbilt University, Nashville, TN USA

Abstract

Modern magnetic resonance imaging (MRI) brain atlases are high quality 3-D volumes with specific structures labeled in the volume. Atlases are essential in providing a common space for interpretation of results across studies, for anatomical education, and providing quantitative image-based navigation. Extensive work has been devoted to atlas construction for humans, macaque, and several non-primate species (e.g., rat). One notable gap in the literature is the common squirrel monkey – for which the primary published atlases date from the 1960's. The common squirrel monkey has been used extensively as surrogate for humans in biomedical studies, given its anatomical neuro-system similarities and practical considerations. This work describes the continued development of a multi-modal MRI atlas for the common squirrel monkey, for which a structural imaging space and gray matter parcels have been previously constructed. This study adds white matter tracts to the atlas. The new atlas includes 49 white matter (WM) tracts, defined using diffusion tensor imaging (DTI) in three animals and combines these data to define the anatomical locations of these tracks in a standardized coordinate system compatible with previous development. An anatomist reviewed the resulting tracts and the inter-animal reproducibility (i.e., the Dice index of each WM parcel across animals in common space) was assessed. The Dice indices range from 0.05 to 0.80 due to differences of local registration quality and the variation of WM tract position across individuals. However, the combined WM labels from the 3 animals represent the general locations of WM parcels, adding basic connectivity information to the atlas.

Keywords

*bennett.landman@vanderbilt.edu; phone 1 (615) 322-2338.

1. INTRODUCTION

Brain atlases are essentially brain anatomies with specific structures labeled in two or three dimensions. With the development of medical imaging technology, magnetic resonance imaging (MRI) brain atlases in three dimensions (3D) have become power tools for neuroscience research [1]. For example, 3D MRI atlases provide a common space for analysis or interpretation of data across studies, the display of 3D brain anatomy for education purposes, and navigation in brain surgery. Extensive work has been devoted to atlas construction for humans, macaque, and several non-primate species (e.g., rats). One notable gap in the literature is the New World (common) squirrel monkey.

The New World squirrel monkey has been used for decades in biomedical research as surrogates for humans and as models for studies of human diseases [2]. Especially in the discipline of neuroscience, the squirrel monkey is thought to be a desirable model because it shares many features of functional organization and microstructural complexity of nervous system with humans and also because it requires less effort to train and handle (e.g., the small size of the squirrel monkey is ideally suited to the narrow bore of an ultra-high filed MRI scanner [3] and requires less histological processing time [4–6]). Published stereotaxic atlases [7, 8] of the squirrel monkey provide labeled cortical structures and white matter regions on 2D photographs of histological sections. Notably, the boundaries of different structures are not labeled and these atlases only cover the middle half of brain, neglecting the prefrontal and occipital lobes. Moreover, the atlases were not readily navigable in 3D, so linkage with modern neuroimaging modalities and visualization techniques is limited.

Recently, a 3D multi-modal MRI atlas of squirrel monkey brain was proposed in [9]. That work defined a common space to best match the printed atlases, created a multi-modal (i.e., anatomical, fractional anisotropy and mean diffusivity) template and delineated several cortical regions based on histological identification. However, the dataset used in the previous study was only from one monkey. To get a more general atlas representing variations of brain anatomy across individuals, we develop a semi-automated iterative process for atlas construction and then build up the brain templates based on datasets from more than seven monkeys. More importantly, white matter (WM) atlases are still not available for the squirrel monkey. Inspired by construction of WM atlases for humans [10] and macaques [11], herein we develop a high resolution 3D WM atlas of the squirrel monkey in the existing common space defined in [9], based on diffusion tenser imaging and tractography.

2. DATA

The squirrel monkey brain MRI data used for atlas construction were acquired in several long-term projects with different ultimate goals. Briefly, all data were collected in a 9.4T, 21 cm bore Agilent scanner. During the *in vivo* session, the live monkey was anaesthetized and its head immobilized. During the *ex vivo* session, the brain, fixed with 4% paraformaldehyde, was placed in phosphate buffered saline in a cylindrical tube for scanning. The scan parameters are listed in Table 1.

3. BRAIN TEMPLATE CONSTRUCTION

Two squirrel monkey brain templates were built in this study. One was based on eight monkeys' *in vivo* anatomical images acquired with a 3D gradient-echo sequence. The other one was based on seven monkeys' *in vivo* anatomical images acquired with 2D gradient-echo multi-slice sequence. The acquisition parameters were listed in Table 1. Image preprocessing included normalizing the image intensity (from the 5th to 95th percentiles), applying a de-noising mask and correcting non-uniform intensity using N4 bias field correction [12].

For each template, the corresponding preprocessed images were registered rigidly to an existing anatomical template created in the atlas' common space [9] using FSL FLIRT [13] with 7 degrees of freedom (DOF) and one of the best aligned images was selected as an initial target. All images were then affine registered to this target using NIFTYReg reg_aladin [14] and an average affine target was computed. Before computing an average, histogram normalization was performed on all images and compared with the normal average of the images. Based on the results, the corresponding method was used in subsequent iterations in computing an average. This average was used as the target for the next iteration and this process was repeated until convergence, producing a final affine target. Figure 1 shows the workflow described above.

The final affine target was used as the initial target for non-rigid registration. Each image was again rigidly registered to the target with 7 DOF. One of the best aligned images was used as the initial target to start the non-rigid registration. All images were registered using ANTS registration tools [15] and then averaged after applying the histogram normalization as needed. This average was used as the target for the next iteration and this process was repeated until convergence, producing the final template of the brain.

4. WHITE MATTER ATLAS CONSTRUCTION

The white matter (WM) atlas was developed based on three monkeys' *ex vivo* diffusion weighted images (DWI) listed in Table 1. The image preprocessing for each monkey included averaging raw DWI data across scans, normalizing intensity and extracting brain tissue from background water (PBS) signal using a homemade script.

4.1 White matter reconstruction

In this step, each brain was processed in its native space. Tensor estimation, seed region selection, deterministic fiber tractography, and fiber tract trimming were performed in DSIStudio (http://dsi-studio.labsolver.org) [16]. Since the WM anatomy of the squirrel monkey is similar to that of the macaque, we used WM regions revealed by histological tracer pathways of the macaque brain [17] as a reference to seed fiber tracking and to refine the tracts (i.e., select, delete and cut) by editing ROIs. The tracking parameters, primarily including termination FA threshold, termination angle threshold, step size and smoothing size, were manually tuned according to the characteristics of each WM bundle. Each WM bundle was tracked, edited and stored as a single 3D fiber density map through DSIStudio. Then the density map was thresholded by custom MATLAB scripts, yielding a binary mask.

The binary mask could be used as a new seed region to repeat the above process iteratively until the quality was acceptable (see Figure 2). The criteria of "good" quality include correctness of 1) the coarse shape and orientation of the WM bundle; 2) the gray matter structures or ventricles next to the WM bundle along the entire pathway and 3) the cortical regions connected by the WM bundle.

Based on WM labels in the squirrel monkey's printed atlases [8, 18] and the WM pathways traced in the macaque's brain [11, 17], 49 distinguishable white matter parcels were identified (including structures with left and right components) for each monkey. Their abbreviations, definitions, primary orientations, seed regions and ROIs for refining tracts are listed in Table 2.

4.2 Registration and normalization

The anatomical brain template created in section 3 was used as a target to perform registration of the WM parcels. Each monkey's non-diffusion weighted volume was registered to the target through affine with 12 DOF followed by non-rigid registration [5, 19] and the deformation field was generated. Then, the binary mask of each WM parcel was transformed into the common space by applying the deformation field. The mask of each specific common white matter parcel was calculated by voting the majority of transformed binary masks across the three monkeys.

4.3 Validation

The created WM parcels for the first monkey in its native space were reviewed by a neuroanatomist with expertise in squirrel monkey brain anatomy. To quantitatively measure the agreement of each WM parcel across the 3 monkeys, the ratio of WM parcels' overlap of 3 monkeys to the WM parcels' union of the 3 monkeys was calculated and denoted by Dice index.

5. RESULTS

The two high resolution anatomical brain templates are shown in Figure 3 and 4. The common WM parcels are illustrated in Figure 5–10. The dice indices for all the WM parcels are in between 5%–81%.

6. CONCLUSIONS AND DISCUSSIONS

In this study, we developed a more general anatomical brain template based on several monkeys and, more importantly, constructed a 3D white matter atlas of the squirrel monkey compatible with the previously defined common MRI space [1] matching the printed atlas. These atlases could be used for locating WM tracts and further for quantitative analysis related to the 3D position of WM tracts in both teaching and research.

One of the sources for lower Dice indices could be local registration errors. Notably, the registration from *ex vivo* individual to *in vivo* brain template is challenging because the brain had significant distortion when put into the cylinder. Another potential source is the variation of the shape as well as the location of the same WM tract across individuals (e.g.,

uncinate fibers). Thus, further work will include improving the registration procedure and adding data from more monkeys to sample more variations across individuals.

Acknowledgments

REFERENCE

1. Toga AW, Thompson PM, Mori S, et al. Towards multimodal atlases of the human brain. Nat Rev Neurosci. 2006; 7(12):952–966. [PubMed: 17115077]

2. Abee CR. The Squirrel Monkey in Biomedical Research. ILAR Journal. 1989; 31(1):11–20.

3. Chen LM, Mishra A, Yang PF, et al. Injury alters intrinsic functional connectivity within the primate spinal cord. Proceedings of the National Academy of Sciences. 2015; 112(19):5991–5996.

4. Gao Y, Choe AS, Stepniewska I, et al. Validation of DTI Tractography-Based Measures of Primary Motor Area Connectivity in the Squirrel Monkey Brain. PloS one. 2013; 8(10):e75065. [PubMed: 24098365]

5. Choe A, Gao Y, Li X, et al. Accuracy of image registration between MRI and light microscopy in the ex vivo brain. Magnetic Resonance Imaging. 2011; 29(5):683–692. [PubMed: 21546191]

6. Schilling K, Janev V, Gao Y, et al. Comparison of 3D orientation distribution functions measured with confocal microscopy and diffusion MRI. Neuroimage. 2016 in press.

7. Emmers, R.; Akert, K. Stereotaxic Atlas of the Brain of the Squirrel Monkey. University of Wisconsin Press; 1963.

8. Gergen, JA.; MacLean, PD. A Stereotaxic Atlas of the Squirrel Monkey's Brain (Saimiri sciureus). U.S. Department of Health, Education, and Welfare; 1962.

9. Gao Y, Khare SP, Panda S, et al. A brain MRI atlas of the common squirrel monkey, Saimiri sciureus. Proceedings of SPIE--the International Society for Optical Engineering. 2014; 9038:90380C–90380C.

10. Wakana S, Jiang H, Nagae-Poetscher LM, et al. Fiber Tract–based Atlas of Human White Matter Anatomy. Radiology. 2004; 230(1):77–87. [PubMed: 14645885]

11. Zakszewski E, Adluru N, Tromp DPM, et al. A Diffusion-Tensor-Based White Matter Atlas for Rhesus Macaques. PLoS ONE. 2014; 9(9):e107398. [PubMed: 25203614]

12. Tustison NG, J. N4ITK: Nick's N3 ITK implementation for MRI bias field correction. Insight Journal. 2009

13. Jenkinson M, Bannister P, Brady M, et al. Improved optimization for the robust and accurate linear registration and motion correction of brain images. NeuroImage. 2002; 17(2):825–841. [PubMed: 12377157]

14. Ourselin S, Roche A, Subsol G, et al. Reconstructing a 3D structure from serial histological sections. Image and Vision Computing. 2001; 19(1–2):25–31.

15. Avants BB, Epstein CL, Grossman M, et al. Symmetric diffeomorphic image registration with crosscorrelation: Evaluating automated labeling of elderly and neurodegenerative brain. Medical Image Analysis. 2008; 12(1):26–41. [PubMed: 17659998]

16. Yeh F-C, Verstynen TD, Wang Y, et al. Deterministic Diffusion Fiber Tracking Improved by Quantitative Anisotropy. PLoS ONE. 2013; 8(11):e80713. [PubMed: 24348913]

17. Schmahmann, J.; Pandya, D. Fiber Pathways of the Brain. Oxford University Press; 2009.

18. Carpenter MB. A stereotaxic atlas of the brain of the squirrel monkey. Archives of Neurology. 1963; 9(1):104–104.

19. Rohde GK, Aldroubi A, Dawant BM. The adaptive bases algorithm for intensity-based nonrigid image registration. IEEE Transactions on Medical Imaging. 2003; 22(11):1470–1479. [PubMed: 14606680]

20. Gao Y, Burns SS, Lauzon CB, et al. Integration of XNAT/PACS, DICOM, and research software for automated multi-modal image analysis. 8674, 867405-867405-7.

21. Harrigan RL, Yvernault BC, Boyd BD, et al. Vanderbilt University Institute of Imaging Science Center for Computational Imaging XNAT: A multimodal data archive and processing environment. NeuroImage. 2016; 124(Part B):1097–1101. [PubMed: 25988229]
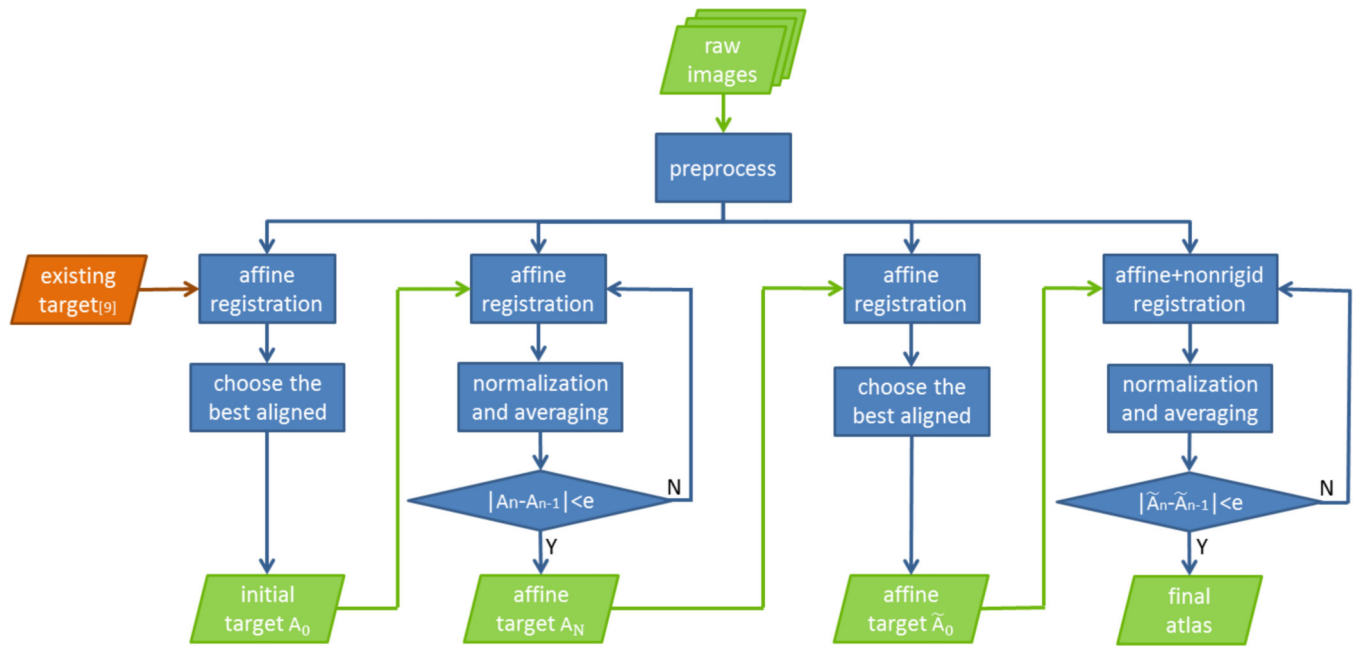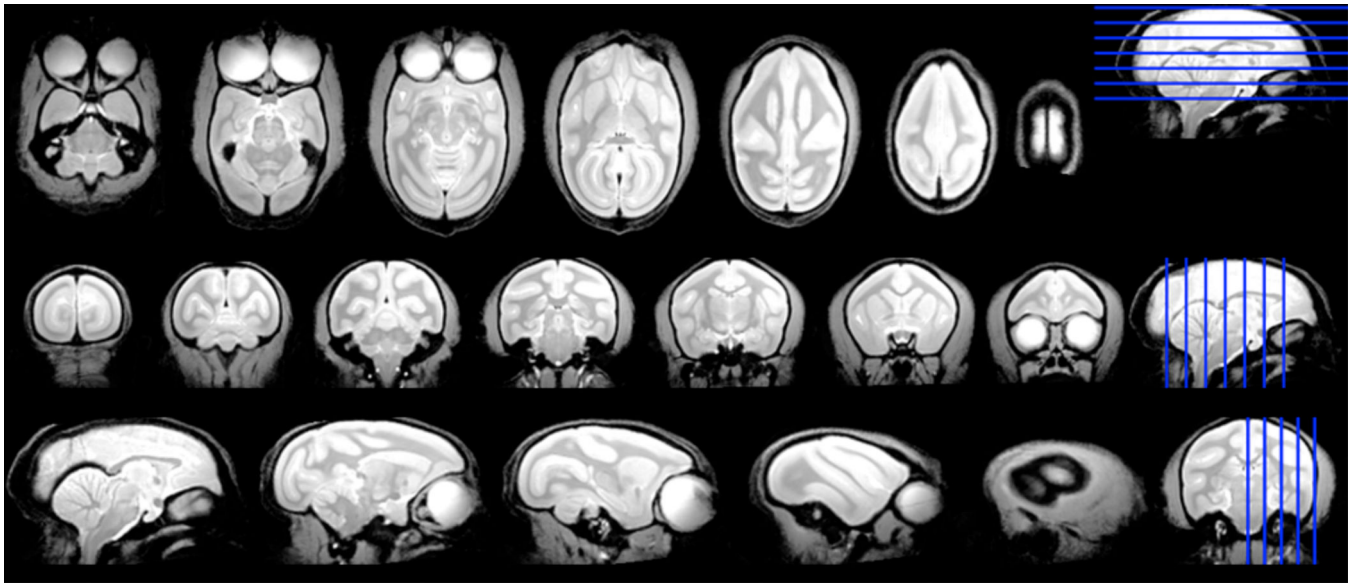
Figure 1.
Flowchart of iterative algorithm to construct anatomical atlas.
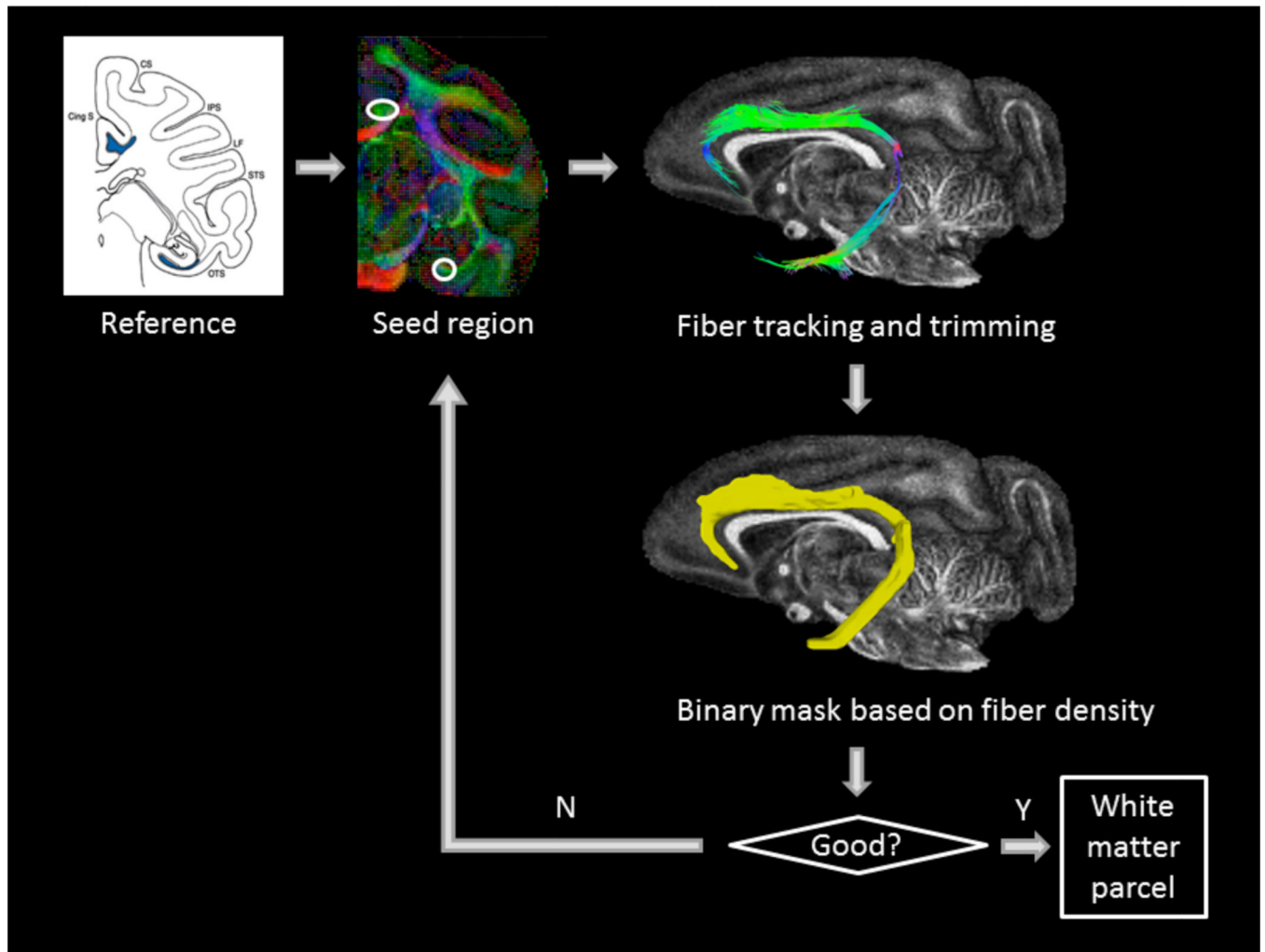
Figure 2.
The pipeline for iterative definition of one bundle – the left cingulum in native space of one monkey. The 'reference' is taken from [17].
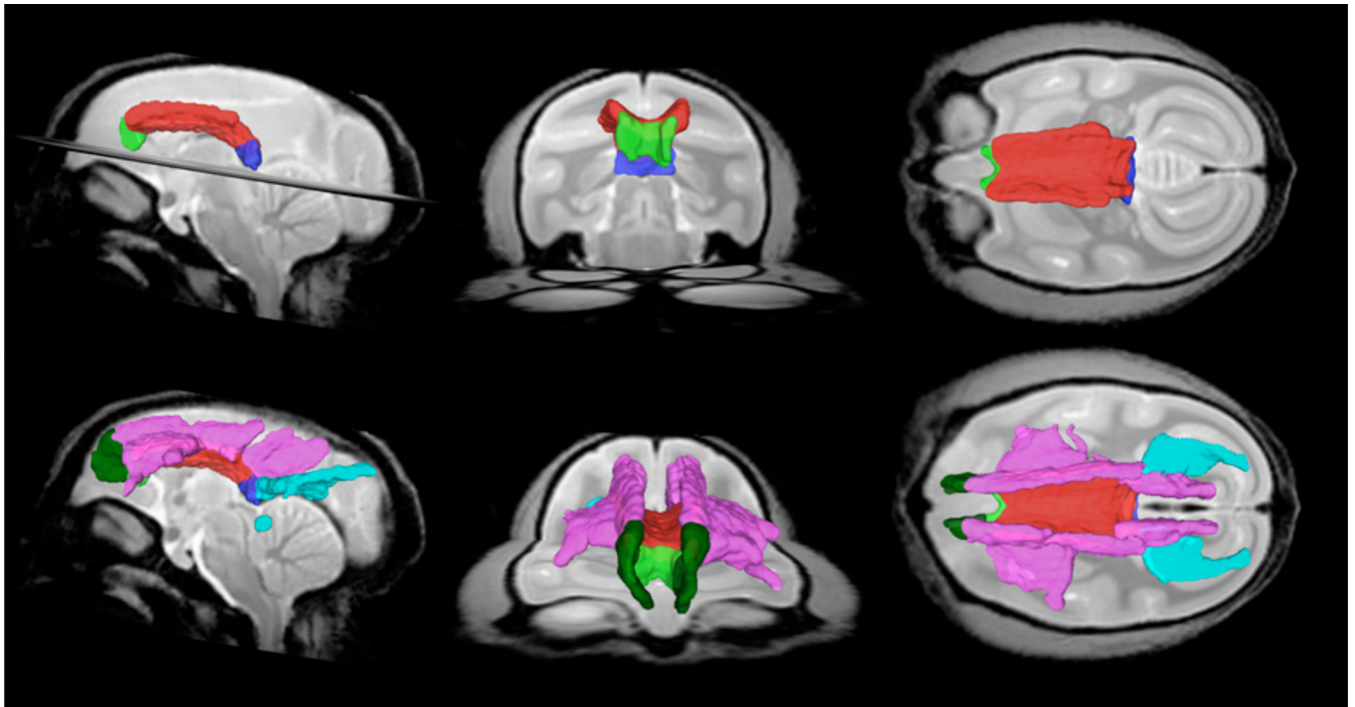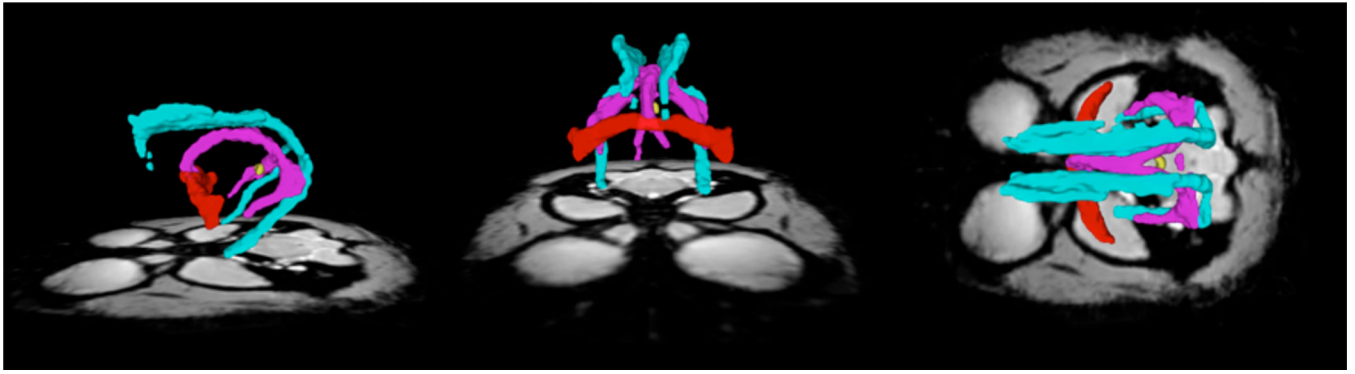
Figure 3.
Axial, coronal and sagittal sections of anatomical monkey brain atlas with $300\times300\times300\mu m^3$ resolution. The images were acquired by gradient echo 3D sequence. The blue lines indicate the locations of the sections on the left side.
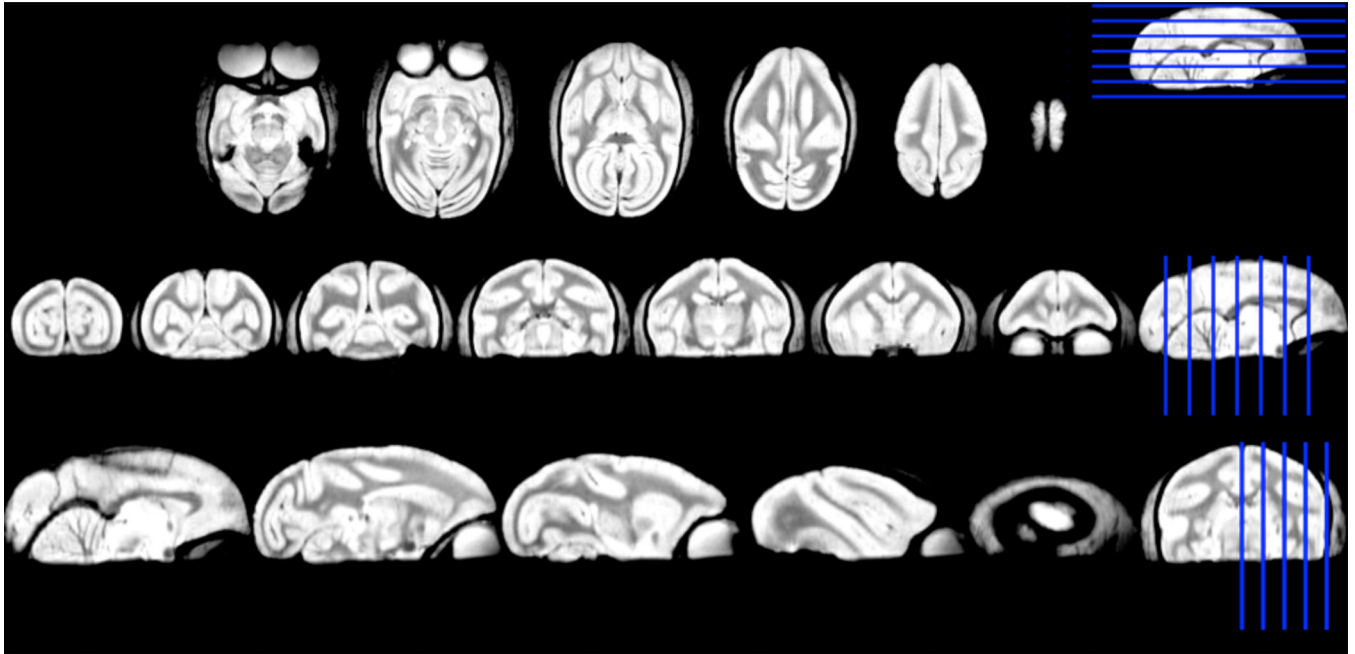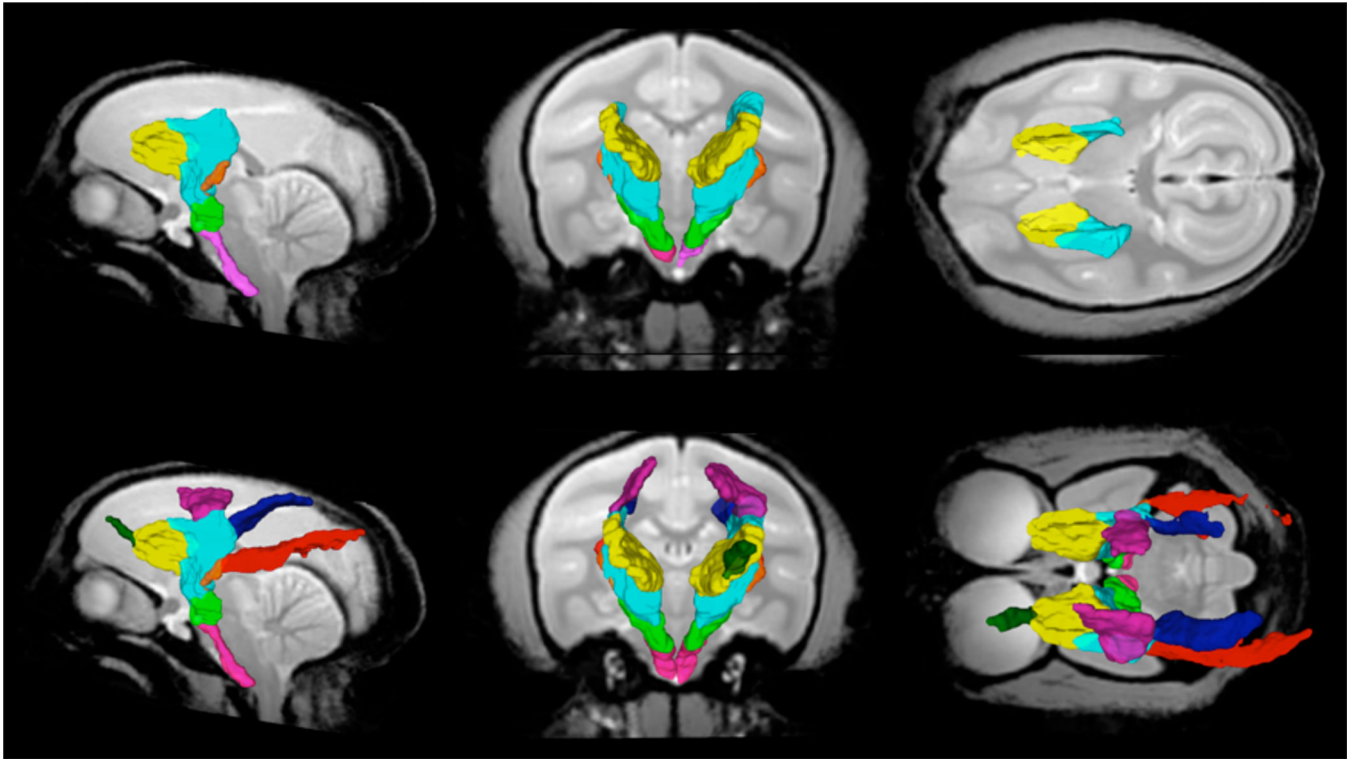
Figure 4.
Axial, coronal and sagittal sections of anatomical monkey brain atlas with $300 \times 300 \times 300 \mu m^3$ resolution. The images were acquired by gradient echo multi-slice sequence. The blue lines indicate the locations of the sections on the left side.
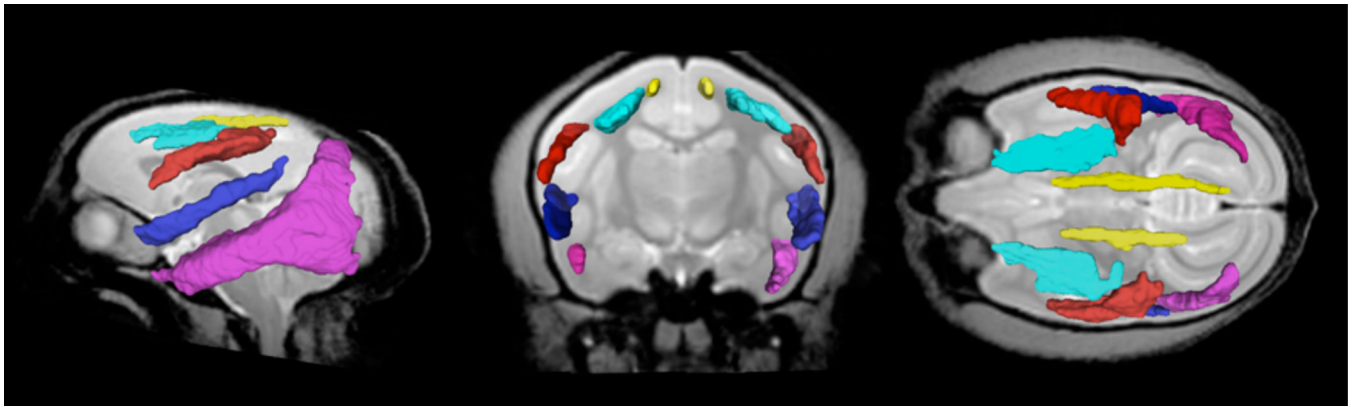
Figure 5.
Sagittal, coronal and axial view of white matter parcels CCg (green), CCb (red), CCs (blue), FCCb (pink), FMn (dark green) and FMj (light blue) in the MRI common space.
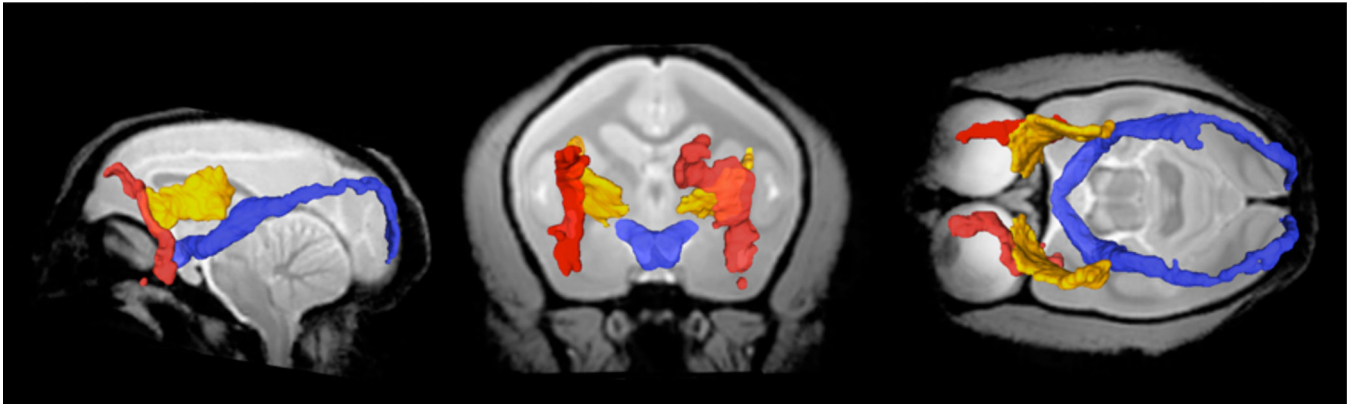
Figure 6.
Sagittal, coronal and axial view of white matter parcels Cing (light blue), F (purple), AC (red) and PC (yellow) in the MRI common space.

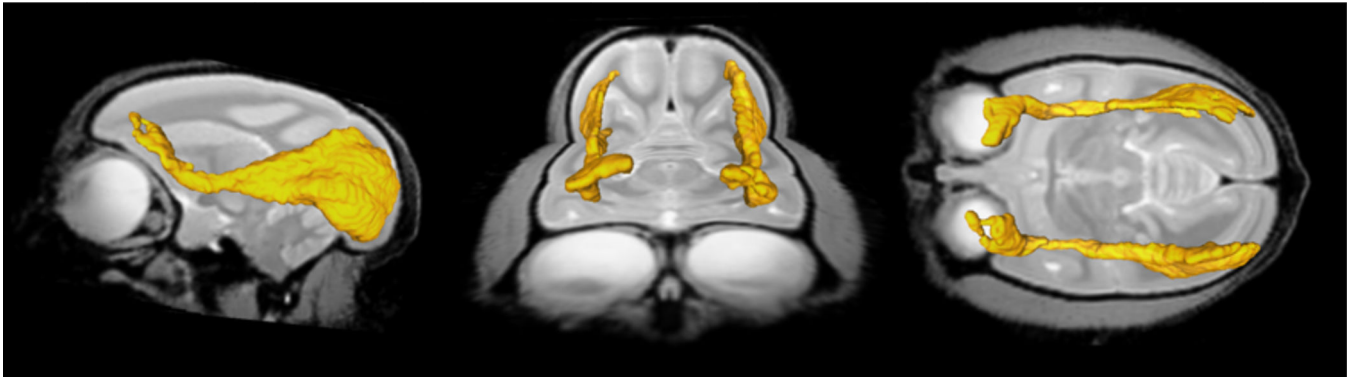**Figure 7.**
Sagittal, coronal and axial view of white matter parcels ICa (yellow), ICg (light blue), ICp (orange), CP (green). CST (pink), CRa (dark green), CRs (purple), CRdp (dark blue) and CRp (red) in the MRI common space.

Figure 8.
Sagittal, coronal and axial view of white matter parcels SLFI (yellow), SLFII (light blue),
SLFIII (red), MLF (blue) and ILF (purple) in the MRI common space.

Figure 9.
Sagittal, coronal and axial view of white matter parcels EC (yellow), UF (red) and IIT (blue) in the MRI common space.

Figure 10.
Sagittal, coronal and axial view of white matter parcels IFOF (yellow) in the MRI common space.

Table 1

List of parameters used in MRI scanning protocols (GEMS: gradient-echo multi-slice; GE3D: gradient echo 3D; SEMSDW: spin-echo multi-slice with diffusion weighting).

	Modality *<sequence>*	Number of monkeys	Scanning parameters
In vivo	anatomical *<GE3D>*	8	TR=5ms, TE=2.4ms, voxel size=500×500×500μm^3, data matrix=128×128×128, flip angle=20°
	anatomical *<GEMS>*	4	TR=600ms, TE=16ms, voxel size=250×250×1000μm^3, data matrix=256×256×24, flip angle=45°
		3	TR=404ms, TE=2.4ms, voxel size=630×630×630μm^3, data matrix=128×128×80, flip angle=20°
Ex vivo	DWI *<SEMSDW>*	3	TR=4.6s, TE=42ms, voxel size=300×300×300μm^3, data matrix=192×128×115, b=0, 1000s/mm^2, number of diffusion gradient directions=30, number of scans>=5, overall scan time=50h

Table 2

List of abbreviation, definition, primary orientation, seed region (S.R.) and constrained ROI of each white matter parcel. (Note: A.: anterior; P.: posterior; L.: left; R.: right; S.: superior; I: inferior, Fasc.: fasciculus)

Abbr.	Definition	Primary Orientation; seed region (S.R.) and other ROIs
SLF I	Superior Longitudinal Fasc. I	A-P; S.R. = most dorsal region with A-P fibers in frontal lobe
SLF II	Superior Longitudinal Fasc. II	A-P; S.R. = lateral region with A-P fibers in frontal lobe
SLF III	Superior Longitudinal Fasc. III	A-P; S.R. = most ventral region with A-P fibers in frontal lobe
MLF	Middle Longitudinal Fasc.	A-P; S.R. = ventral region with A-P fibers in superior temporal lobe
ILF	Inferior Longitudinal Fasc.	A-P; S.R. = ventral region with A-P fibers in inferior temporal lobe
IFOF	Inferior Fronto-Occipital Fasc.	A-P; S.R. = entire white matter region of one coronal slice in occipital lobe; terminating region = prefrontal area
UF	Uncinate Fasc.	A-P; S.R. = ventral region with A-P fibers in inferior temporal lobe
Cing	Cingulum	A-P; S.R. = region between cingulate and corpus callosum with A-P fibers
F	Fornix	A-P; S.R. = region underneath corpus callosum with A-P fibers
ICa	Internal Capsule -anterior limb	S-I/A-P; S.R. = anterior limb of internal capsule with A-P fibers
ICg	Internal Capsule-genu	S-I; S.R. = genu limb of internal capsule with S-I fibers
ICr	Internal Capsule -retrolenticular limb	A-P; S.R. = retrolenticular limb internal capsule with A-P fibers
CRa	Coronal Radiata-anterior	A-P; S.R. = ICa; terminating region = prefrontal lobe;
CRs	Coronal Radiata-superior	S-I; S.R. = ICg; terminating region = frontal lobe
CRdp	Coronal Radiata -dorsal posterior	S-I; S.R. = ICg; terminating region = parietal lobe
CRp	Coronal Radiata-posterior	A-P; S.R. = ICr; terminating region = occipital lobe
CCg	Corpus callosum-genu	L-R; S.R. = the middle sagittal slice of corpus callosum with L-R fibers; terminating ROI = prefrontal lobe
CCb	Corpus callosum-body	L-R; S.R. = the middle sagittal slice of corpus callosum with L-R fibers; terminating ROI = frontal and parietal lobe
CCs	Corpus callosum-splenium	L-R; S.R. = the middle sagittal slice of corpus callosum with L-R fibers; terminating ROI = occipital lobe
FMn	Forceps Minor	A-P; S.R. = CCa; terminating lobe = prefrontal lobe
FCCb	Fiber extension of CCb	S-I and L-R; S.R. = CCb; terminating ROI = frontal and parietal lobe
FMj	Forceps Major	A-P; S.R. = CCs; terminating ROI = occipital lobe
AC	Anterior Commissure	L-R; S.R. = middle sagittal slice of AC with L-R fibers running
PC	Posterior Commissure	L-R; S.R. = middle sagittal slice of PC with L-R fibers running
IIT	Optic tract	A-P; S.R. = optic chiasm with L-R fibers in frontal lobe
EC	External and Extreme Capsule	A-P; S.R. = region lateral to lentiform nucleus with A-P fibers